Available online at www.sciencedirect.com

SciVerse ScienceDirect

Energy Procedia 34 (2013) 617 – 626

Energy Procedia

10th Eco-Energy and Materials Science and Engineering
(EMSES2012)

Photoelectrochemical Properties of WO_3 Thin Films Prepared by Electrodeposition

W.L. Kwong, H. Qiu, A. Nakaruk, P. Koshy, and C.C. Sorrell*

School of Materials Science and Engineering
University of New South Wales, Sydney, NSW 2052, Australia

Abstract

Tungsten trioxide (WO_3) thin films were synthesised by electrodeposition using peroxotungtic acid as the precursor electrolyte solution for use as photoanodes in a photoelectrochemical cell for solar hydrogen applications. The films were coated at deposition potentials varying from –0.30 to –0.90 V versus Ag/AgCl in order to study the effect of the potential on the mineralogical, morphological, optical, and photoelectrochemical properties of the nanoparticulate films.

The films were composed of monoclinic WO_3, the degree of crystallinity and preferred orientation of the orthogonal planes of which increased with deposition potential and associated film thickness. In contract, increasing the deposition potential had a minimal impact on the particle sizes, which were in the range ~80-90 nm. While films deposited at the potential range of –0.30 to –0.60 V showed controlled nanostructures with thicknesses in the range 168-431 nm, increasing the deposition potential from –0.70 to –0.90 V resulted in rapid increase in film, which led to cracking from drying stress. Linear voltammetry data suggested that the optimal potential for the deposition of stable films was in the range –0.37 to –0.60 V. However, the data for the film deposited at a potential of –0.30 V indicated a film of high quality. Further, the data for the film deposited at a potential of –0.60 V indicated a film of a low quality and so this voltage represents a transition point for stable-unstable film growth and unstressed-stressed nanostructure from drying. The trends in the optical transmission properties showed that the photocatalytic activity of the films could be expected to decrease with increasing potential, thickness, and crystallinity. That is, the band gap and projected absorption edge exhibited a red shift. This was attributed to the relative effects of the surface and volume band gaps, in which the latter would increase relative to the former with increasing thickness.

The photocurrent densities reflected the effects of increasing solid volume and decreasing band gap with increasing film thickness. The exception was the reduced performance of the film deposited at the potential of –0.60 V. This outcome was attributed to the competition between the photogeneration and recombination of electron-hole pairs, where the potential of –0.60 V represents the transition point described above.

Selection and peer-review under responsibility of COE of Sustainalble Energy System, Rajamangala University of Technology Thanyaburi (RMUTT)

Keywords: Tungsten Oxide, Electrodeposition, Deposition Potential, Thin Films, Photoelectrochemical Properties

* Corresponding author. Tel.: +61 (0)2 9385 4421; fax: +61 (0)2 9385 6565.
E-mail address: c.sorrell@unsw.edu.au.

Selection and peer-review under responsibility of COE of Sustainalble Energy System, Rajamangala University of Technology Thanyaburi (RMUTT)
doi:10.1016/j.egypro.2013.06.793

1. Introduction

Photoelectrochemical solar-hydrogen can be produced by the conversion of solar energy to chemical energy, which is stored in the form of hydrogen fuel. This process is environmentally clean and renewable and the principle involves the photogeneration of excitons by photosensitive semiconductor materials. These photogenerated holes and electrons oxidise and reduce water molecules, respectively, to produce oxygen and hydrogen gases, respectively, at separate electrodes of a photoelectrochemical cell [1]. In a fuel cell, the oxidation of hydrogen generates almost triple the energy obtained from fossil fuels, with water being the by-product [2,3]. The route used to synthesise semiconductor photoelectrodes is important because it determines the performance of the photoelectrochemical cell. During the past few decades, tungsten oxide (WO_3) has become an important candidate for use as a photoanode owing to its high resistance against corrosion and photocorrosion [4] as well as its ability to absorb visible light (having a relatively small optical band gap) [5,6].

The practical implementation of WO_3 photoanodes often is in the form of thin films owing to better processing flexibility and lower costs. Numerous synthesis techniques have been used to produce WO_3 thin films and these include sol-gel [7], electrochemical anodisation [8], hydrothermal/solvothermal [9], cathodic electrodeposition [10], spray pyrolysis [11], magnetron sputtering [12] and thermal oxidation [13]. Of these techniques, electrodeposition is advantageous due to the following [14]:

1) Excellent possibility of direct coating of films on large-area conductive substrates
2) Simple and low-cost process, which enables large-scale production
3) Good potential for controlling film thickness by monitoring charge consumption during deposition

The physical properties of WO_3 thin films have been demonstrated to be controllable by varying the processing conditions of electrolyte solution chemistry [10,15], during deposition [16,17], and post-deposition [18,19]. In other words, careful choice of the deposition parameters is important to control the properties of WO_3 thin films and to ensure that these films are crack-free and highly crystalline and that they possess the optimal photoelectrochemical properties. The present work describes the effect of the deposition potential (voltage) on the deposition mechanisms and the resultant mineralogical, morphological, and optical properties of electrodeposited tungsten oxide thin films. The influence of these characteristics on the photoelectrochemical performance of these thin films also is analysed.

2. Experimental Procedure

2.1. Preparation of thin films

Tungsten oxide thin films were electrodeposited from peroxotungstic acid (PTA) solutions, which were prepared by dissolving tungsten foil in hydrogen peroxide. The excess hydrogen peroxide (H_2O_2), formed upon complete dissolution of the tungsten foil, was eliminated catalytically by immersing a platinum foil into the solution. The decomposition of excess H_2O_2 was accelerated by heating the solution to 70°C until gas evolution ceased. Clear yellow solutions of PTA were obtained by this procedure. The solutions were diluted to 0.05 $mol \cdot L^{-1}$ (metal basis) by adding propan-2-ol and these were used as the electrolyte solutions for deposition. The pH value of the solution was 2.14 at room temperature.

A standard three-electrode electrochemical cell was employed for the sample deposition. A fluorine-doped tin oxide (FTO) substrate, Pt foil, and Ag/AgCl were used as the working, counter, and reference electrodes, respectively. All reported potential values are in relation to the reference electrode. The electrochemical cell was controlled using a potentiostat connected to a computer for datalogging. Prior to film deposition, a linear potential sweep was conducted at a scan rate of 5 $mV \cdot s^{-1}$ and a step size of 1 mV. The depositions were done at room temperature at deposition potentials varying from –0.3 V to –0.6 V for a fixed deposition time of 90 min. The as-deposited samples were rinsed with distilled water, dried in air, and annealed in a muffle furnace at 450°C for 2 h in air (heating and initial cooling rates were $5°C \cdot min^{-1}$).

2.2. Characterisation of the films

The mineralogical analyses of the films were done using *in situ* X-ray powder diffraction (Philips X'pert Materials Powder Diffractometer, CuKα radiation, 45 kV, 40 mA). The surface morphologies of the films were assessed using scanning electron microscopy (FEI Nova NanoSEM, accelerating voltage 5 kV). The film thicknesses were determined by focused ion beam milling (XT Nova Nanolab 200), followed by cross-sectional viewing at an angle of 45° using the NanoSEM. A UV-Visible spectrophotometer (Pelkin-Elmer Lambda 35) was used to measure the optical transmittances of the films in the wavelength region of 250 nm to 800 nm.

The same electrochemical system described above was employed for the photoelectrochemical measurements of the films. WO_3 films on FTO substrates and 0.5 $mol \cdot L^{-1}$ NaCl aqueous solution (pH = 6.27) were used as the working electrode and electrolyte, respectively. The light source was a 50 W tungsten-halogen lamp of intensity ~30 $mW \cdot m^{-2}$ (measured using a Digitech QM1587 light meter, light source-sample distance ~45 cm), chopped at a frequency of 0.05 Hz.

3. Results and Discussion

PTA solutions without hydrogen peroxide were unstable. Precipitation was observed readily when the PTA solutions were heated beyond the point at which gas evolution ceased and/or after a day of storage at room temperature. The instability of PTA solutions has been reported elsewhere [20,22] and the precipitate was identified as tungstic acid [22]. The addition of propan-2-ol improved the lifetime of PTA solutions and enabled their storage for more than three days without any precipitate formation.

Figure 1 shows the linear sweep voltammogram for the PTA electrolyte solution of 0.05 $mol \cdot L^{-1}$ W concentration. The dashed lines at approximately –0.37 V and –0.60 V, corresponding approximately to the flattest portion of the curve, delineate the optimal potential range for the reduction of the PTA ions to tungsten oxide [23,24], as indicated by consistent quality of the films (–0.37 V represents the minimal deposition potential required to reduce the PTA ions to tungsten oxide).

Figure 2(a) shows the SEM surfaces and cross-sectional images (insets) of the annealed films deposited at different voltages. The films consisted of irregularly shaped particles that formed a porous network. The film thicknesses (and hence the deposition rates) increased from 168 nm to 431 nm with increasing potential. The average particle sizes of the matrix grains were in the range ~80-90 nm and the variations were insignificant at different deposition potentials, indicating that the nucleation and growth mechanism is not influenced significantly by the variation of deposition potential. However, the sample deposited at −0.60 V, which is the thickest of the four, exhibited some exaggerated grain growth. This potential lies at the upper limit of the range for stable film growth, as shown in Figure 1.

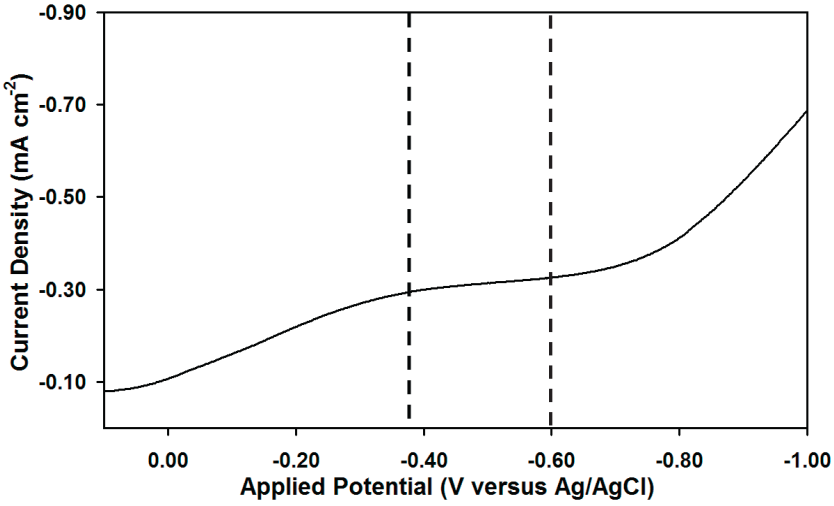

Fig. 1. Linear sweep voltammogram in peroxotungstic acid solution of 0.05 mol·L^{-1} tungsten

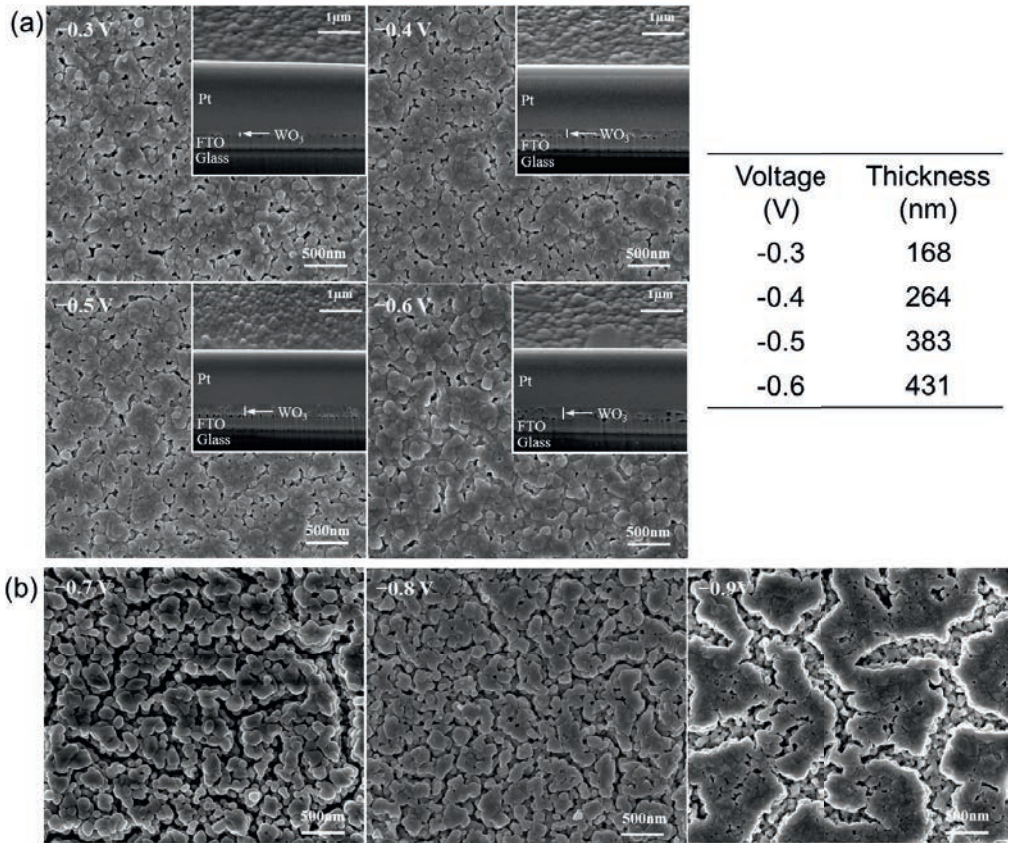

Voltage (V)	Thickness (nm)
-0.3	168
-0.4	264
-0.5	383
-0.6	431

Fig. 2. SEM images of the annealed films deposited at (a) –0.3 V to –0.6 V and (b) –0.7 V to –0.9 V

Increasing the deposition potential enhances the electric field strength between the working (FTO substrate) and the counter (Pt foil) electrodes and this accelerates the transport of the PTA ions for deposition at the FTO substrates, as evidenced by the overall increasing current density shown in Figure 1. The rapid increase in current density above –0.60 V generated films of thickness >634 nm, without significant difference in matrix particle size, and this resulted in excessive drying shrinkage and potential cracking, as shown in Figure 2(b). Hence, the potential of –0.60 V also represents the upper limit to produce films of sufficient thinness to avoid drying shrinkage stresses.

The as-deposited films were amorphous, as confirmed by the characteristic broad peaks in the XRD patterns (not shown). Crystallisation of the films upon annealing was confirmed by the XRD spectra shown in Figure 3. Three major diffraction peaks at 2θ angles of ~ 23.1°, 23.6°, and 24.3° represent the (002), (020), and (200) planes, respectively, for monoclinic WO_3 [25]. Some preferred crystal plane growth of the (002) and (200) planes can be seen (all three peaks are of approximately equal intensities in random orientation), as has been observed by others [10,26]. It is likely that this resulted from the easier growth of the orthogonal planes (002) and (200) relative to the non-orthogonal plane (020). The general increased peak intensities with deposition potentials are attributed to improved crystal lattice symmetry as the film grew and increased in thickness, as shown in Figure 2(a), which was associated with the relief of physical mismatch stresses at the film/substrate interface.

Figure 4 shows the optical transmittance spectra of the annealed films deposited at various potentials. It can be seen that the transmittance of the films deposited at –0.3 V to –0.5 V were fairly constant (~70%) in the wavelength range of >400 nm. The relatively low transmittance in the same wavelength range of the film deposited at –0.6 V, which probably results from this potential representing a transition point for both stable growth and film thinness.

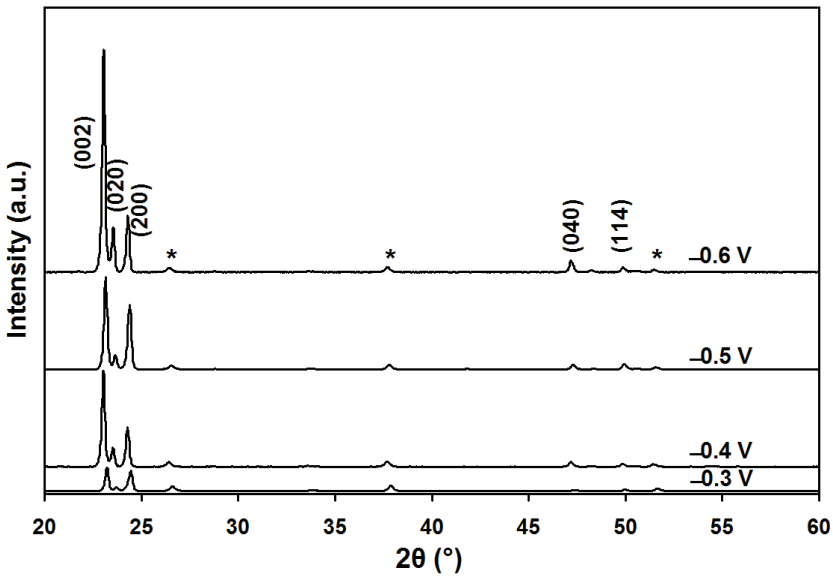

Fig. 3. XRD spectra of the annealed films deposited at various potentials (* indicates peaks of FTO substrate)

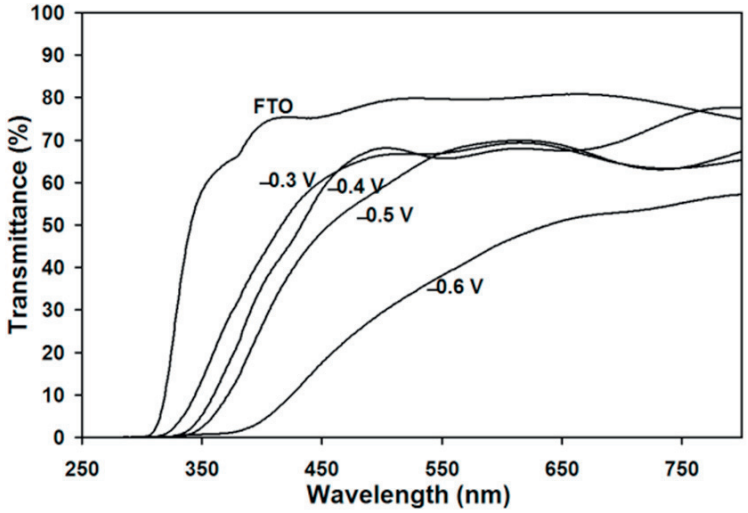

Voltage (V)	Band gap (eV)
-0.3	2.96
-0.4	2.95
-0.5	2.85
-0.6	2.50

Fig. 4. Optical transmittance spectra as a function of wavelength of the annealed films deposited at various potentials

In addition, the transmission of the films shifted to longer wavelengths with increasing deposition potential. Also, the transmission of the film deposited at –0.6 V was significantly lower than those of the three thinner films. The reason for the former is that the optical indirect band gap consists of contributions from both the surface and volume band gaps, where the former usually is larger with thicker films [15]. More specifically, the reason for the latter is that it is well known that such transmission curves are associated with high concentrations of grain boundary defects that serve as electron-hole recombination sites [26]. Consequently, the concentration of surface defects (relative to the total volume), which provide surface-active sites for photocatalysis, remains nearly constant while the volume, which contains recombination sites at the grain boundaries, continues to increase as the film thickness increases.

The optical indirect band gaps of the films were estimated using the method of Tauc and Menth [27]:

$$(\alpha h\nu)^{1/2} = C(h\nu - E_g) \quad (1)$$

Where: $\alpha = -(1/d)\ln(T/100)$
d = Film thickness
T = Optical transmittance
h = Planck's constant
ν = Frequency of light
C = Constant
E_g = Optical indirect band gap

The values of the optical indirect band gap (E_g) were estimated from extrapolation from the absorption edge to the abscissa of the plot of $(\alpha h\nu)^{1/2}$ versus $h\nu$. The E_g values of the films were in the range 2.50-2.96 eV, where they decreased with increasing deposition potential. Again, this variation can be attributed to the surface/volume defect considerations. Another issue related to the expected photocatalytic performance of these films is the increasing crystallinity and decreasing physical mismatch stress with increasing film thickness (where impurity, particle size, and roughness effects are irrelevant or minimal for these nanostructures). In this case, the greater crystallinity with the thicker films equates to a reduction in the defect concentration, especially at the surface, and so the photoactivity would be expected to decrease with increasing thickness.

Figure 5 shows the photocurrent densities of the films measured under chopped illumination and at a fixed applied potential of 0.70 V. The photocurrent densities dropped to nearly zero when the illumination was chopped off and rose instantly when the films were illuminated. It can be seen that the photocurrent density increased with increasing deposition potentials of –0.30 V to –0.50 V. This is attributed to improved light absorption at longer wavelengths owing to the decreasing optical indirect band gaps, which enhances the photogeneration of electron-hole pairs for water photolysis. However, a lower photocurrent density was obtained for the film deposited at the higher potential of –0.60 V, despite its relatively low optical band gap. This is attributed to the competing mechanisms of photogeneration and recombination of electron-hole pairs. Since the potential of –0.60 V represents the transition to unstable film growth and drying shrinkage stresses, this nanostructure was likely to have been more defective than those deposited at lower potentials. Hence, these defects are equated with recombination sites.

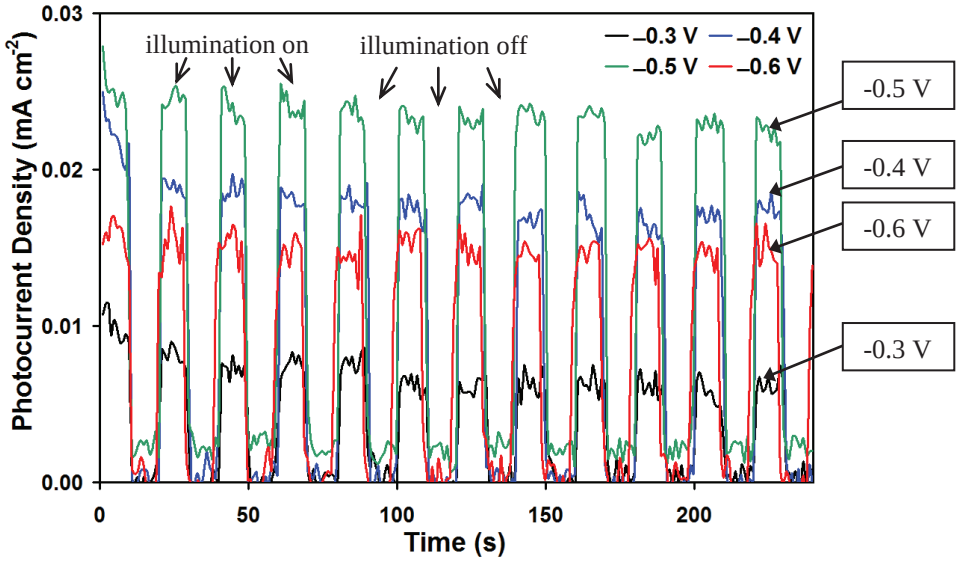

Fig. 5. Potentiostatic photocurrent densities of the annealed films measured under chopped illumination at 0.7 V *vs* Ag/AgCl in 0.5 mol·L^{-1} NaCl aqueous electrolyte

4. Conclusions

The effects of the deposition potential on the mineralogical, morphological, optical, and photoelectrochemical properties of electrodeposited WO_3 thin films, electrodeposited from peroxotungstic acid (PTA) solutions, were investigated. The resultant nanostructures showed an average matrix particle size in the range ~80-90 nm and thicknesses in the range 168-431 nm. The WO_3 was monoclinic and there appeared to be preferred growth of the orthogonal planes.

While increasing the deposition potential insignificantly affected the particle sizes, the deposition kinetics tended to increase, leading to rapid growth in the thickness of the films. The films were comprised of monoclinic WO_3, which increased in crystallinity with increasing thickness owing to reduction in physical mismatch stress.

A range of potentials (–0.30 V to –0.90 V) was used for film deposition. The linear sweep voltammetry data suggest that a range of –0.37 V to –0.60 V is optimal for film growth. However, the film deposited at a potential of –0.30 V appeared to be of good quality. In contrast, the deposition potential of –0.60 V appears to represent a transition between stable and unstable film growth as well as a transition between films undamaged and damaged by drying stress.

The optical transmission data revealed relatively high transmissions and low optical indirect band gaps for the films deposited at the potential range of –0.30 V to –0.50 V, with a red shift with increasing potential, associated film thickness, and crystallinity. The film deposited at the potential of –0.60 V revealed a curve consistent with a highly defective material. This trend is consistent with the relative effects from surface and volume defect conditions and associated band gaps. The significant degradation in the film deposited at the potential of –0.60 V is likely to have resulted from the fact that it represents the transition to unstable film growth and onset of drying stress.

The photocurrent densities were consistent with the effect of increasing solid volume and decreasing band gap as a function in increasing thickness, except for the film deposited at the potential of –0.60 V, which showed inferior performance. In this case, the effect was attributed to the competition between the photogeneration and recombination of electron-hole pairs, where the transition to unstable growth and residual stress suggest a significant enhancement of the defects enhancing recombination.

Acknowledgements

This work was supported in part by a project funded by the Australian Research Council (ARC). The authors are grateful for the characterisation facilities provided by the Australian Microscopy & Microanalysis Research Facilities (AMMRF) node at the University of New South Wales (UNSW). H. Qiu is grateful for Postgraduate Research Support Scheme funding to attend the conference at which this work was presented.

References

[1] Miller EL. On Solar Hydrogen and Nanotechnology. Singapore: John Wiley and Sons; 2009.

[2] Grimes CA, Varghese OK, Ranjan S. Light, Water, Hydrogen. The Solar Generation of Hydrogen by Water Photoelectrolysis. New York: Springer Science+Business Media; 2008.

[3] Wallner T. Correlation between speciated hydrocarbon emissions and flame ionization detector response for gasoline/alcohol blends. *J Eng Gas Turbines Power* 2011;**133**:082801.

[4] Hodes G, Cahen D, Manassen J. Tungsten trioxide as a photoanode for a photoelectrochemical cell (PEC). *Nature* 1976;**260(5549)**:312-13.

[5] Hanaor DAH, Triani G, Sorrell CC. Morphology and photocatalytic activity of highly oriented mixed phase titanium dioxide thin films. *Surf Coat Technol* 2011; **205**:3658-664.

[6] Nakaruk A, Ragazzon D, Sorrell CC. Anatase–rutile transformation through high-temperature annealing of titania films produced by ultrasonic spray pyrolysis. *Thin Solid Films* 2010;**518**:3735-742.

[7] Solarska R, Alexander BD, Braun A, Jurczakowski R, Fortunato G, Stiefel M et al.. Tailoring the morphology of WO_3 films with substitutional cation doping: effect on the photoelectrochemical properties. *Electrochim Acta* 2010, **55(26)**:7780-787.

[8] Ng C, Ye CH, Ng YH, Amal R. Flower-shaped tungsten oxide with inorganic fullerene-like structure: synthesis and characterization. *Crys Growth Des* 2010;**10**:3794-801.

[9] Amano F, Li D, Ohtani B. Fabrication and photoelectrochemical property of tungsten (VI) oxide films with a flake-wall structure. *Chem Comm* 2010;**46**:2769-771.

[10] Yang B, Li HJ, Blackford M, Luca V. Novel low density rnesoporous WO_3 films prepared by electrodeposition. *Curr Appl Phys* 2006;**6**:436-39.

[11] Sun Y, Murphy CJ, Reyes-Gil KR, Reyes-Garcia EA, Thornton JM, Morris NA, Raftery D. Photoelectrochemical and structural characterization of carbon-doped WO_3 films prepared via spray pyrolysis. *Int J Hydrogen Energy* 2009;**34**: 8476-484.

[12] Cole B, Marsen B, Miller E, Yan YF, To B, Jones K, Al-Jassim M. Evaluation of nitrogen doping of tungsten oxide for photoelectrochemical water splitting. *J Phys Chem C* 2008;**112**:5213-220.

[13] Wang H, Quan X, Zhang Y, Chen S. Direct growth and photoelectrochemical properties of tungsten oxide nanobelt arrays. *Nanotechnol* 2008;**19**:065704.

[14] Fulop GF, Taylor RM. Electrodeposition of semiconductors. *Annu Rev Mater Sci* 1985;**15**:197-210.

[15] Kwong WL, Savvides N, Sorrell CC. Electrodeposited nanostructured WO_3 thin films for photoelectrochemical applications. *Electrochim Acta* 2012;**75**:371-80.

[16] Baeck SH, Jaramillo T, Stucky GD, McFarland EW. Controlled electrodeposition of nanoparticulate tungsten oxide. *Nano Lett* 2002;**2(8)**:831-34.

[17] Soliman HMA, Kashyout AB, El Nouby MS, Abosehly AM. Preparation and characterizations of tungsten oxide electrochromic nanomaterials. *J Mater Sci-Mater Electron* 2010;**21(12)**:1313-321.

[18] Deepa M, Srivastava AK, Agnihotry SA. Influence of annealing on electrochromic performance of template assisted, electrochemically grown, nanostructured assembly of tungsten oxide. *Acta Mater* 2006;**54**:4583-595.

[19] Deepa, M.; Srivastava, A.K.; Saxena, T.K.; and Agnihotry, S.A. Annealing induced microstructural evolution of electrodeposited electrochromic tungsten oxide films. *Appl Surface Sci* 2005;**252**:1568-580.

[20] Shen, P.K.; and Tseung, A.C.C. Study of electrodeposited tungsten trioxide thin films. *J Mater Chem* 1992; **2(11)**:1141-147.

[21] Shen, P.K.; Syed-bokhari, J.; and Tseung, A.C.C. The performance of electrochromic tungsten trioxide films doped with cobalt or nickel. *J Electrochem Soc* 1991;**138(9)**:2778-783.

[22] Yamanaka K. Electrodeposited films from aqueous tungstic acid-hydrogen peroxide solutions for electrochromic display devices. *Jpn J Appl Phys* 1987;**26(11)**:1884-890.

[23] Bijani S, Martínez L, Gabás M, Dalchiele EA, Ramos-Barrado J-R. Low-temperature electrodeposition of Cu_2O thin films: modulation of micro-nanostructure by modifying the applied potential and electrolytic bath pH. *J Phys Chem C* 2009;**113**:19482-19487.

[24] Wu L, Tsui L-K, Swami N, Zangari G. Photoelectrochemical stability of electrodeposited Cu_2O films. *J Phys Chem C* 2010; **114**: 11551-1556.

[25] Woodward PM, Sleight AW, Vogt T. Structure refinement of triclinic tungsten trioxide. *J Phys Chem Solids*; 1995, **56(10)**: 1305-315.

[26] Zook JD. Effects of grain boundaries in polycrystalline solar cells. *Appl Phys Lett* 1980;**37(2)**: 223-26.

[27] Tauc J, Menth A. States in the gap. *J Non-Cryst Solids* 1972; **8-10**:569-85.